Bioengineered protein nanocage by small heat shock protein delivering mTERT siRNA for enhanced colorectal cancer suppression

Hao Wang[1,2], Ning Liu[2], Fuxu Yang[1, 2], Nannan Hu[1,2], Mingyue Wang[2], Meiying Cui[2], Nico Bruns[3], Xingang Guan[*,1,2]

[1]Medical College, Taizhou University, 1139 Shifu Avenue, Taizhou 318000, PR China.

[2]College of Medical Technology, Beihua University, 3999 East Binjiang Road, Jilin 132013, PR China

[3]Department of Pure and Applied Chemistry, University of Strathclyde, 295 Cathedral Street, Glasgow G1 1XL, UK

*Corresponding author： guanxg@ciac.ac.cn

Keywords: protein nanocage; siRNA delivery; RGD; TERT; cancer therapy

Abstract:

Efficient delivery of small interfering RNA (siRNA) for target gene silence holds great promise for cancer therapy. Protein nanocages have attracted considerable attention as ideal drug delivery systems because of material-derived advantages and unique structural properties. However, most studies about siRNA delivery have not indicated the real role of protein nanocages in inhibiting tumor growth in vivo. Herein, we fabricated an efficient siRNA delivery system using the small heat shock protein (Hsp) nanocage decorated with Arg-Gly-Asp (RGD) and transactivator of transcription (Tat) peptide. Hsp-Tat-RGD NC showed good cellular uptake and lysosomal escape in colorectal cancer cells. In addition, the nanocage could efficiently transfect siRNA into the cytoplasmic area of CT26 cells. Hsp-Tat-RGD NC delivering telomerase reverse transcriptase (TERT)-targeting siRNA could significantly downregulate TERT protein expression and trigger tumor cell apoptosis in vitro. More importantly, Hsp-Tat-RGD/siTERT complexes nearly completely inhibited the tumor growth after five times of treatment in mice bearing CT26 xenograft. Our results demonstrate the great potential of Tat/RGD-decorated Hsp nanocage as a promising siRNA delivery platform for cancer therapy.

Introduction

Nowadays, colorectal cancer (CRC) ranks the second leading cause of cancer death worldwide in 2020, with an estimated 1.93 million new cases and 0.94 million deaths reported.[1,2] The high metastasis (20~25%) and post-surgical recurrence (about 50%) collaboratively contribute to the poor prognosis of CRC. Less than 20% of a 5-year

survival rate is obtained.[3,4] Although conventional chemotherapeutics have prolonged the overall survival of CRC patients, the severe side effects such as sensory neuropathy, diarrhea, and alopecia greatly limit their further clinic application.[5] Safe and effective formulations are of great significance for the improved efficacy of advanced CRC.

Recently, many reports have shown improved outcomes by silencing critical genes for maintaining tumor cell growth, metastasis, angiogenesis, or inhibiting apoptosis.[6] Telomerase comprises RNA component and catalytic subunit telomerase reverse transcriptase (TERT) maintains telomere length.[7-9] TERT gene expression is strictly regulated in adult somatic cells, while increased TERT expression is detected in some solid cancers.[10,11] The upregulated TERT protein leads to enhanced telomerase activity and participates in the immortal properties of cancer cells.[12] Nowadays, the promoter mutations in the TERT gene function as a potential biomarker for cancer diagnosis and prognosis.[13,14] Therefore, targeted TERT regulation represents a promising therapeutic strategy for effective cancer treatment.[15,16]

RNA interference (RNAi) is a cutting-edge technology for silencing target genes using short hairpin RNA (shRNAs) or small interfering RNA (siRNA).[17] RNAi therapies have shown tremendous potential in the treatment of some diseases.[18] However, the therapeutic efficacy through RNAi is mainly determined by the delivery efficiency of RNAi drugs to target cells due to the easy degradation of RNA in vivo.[19] In addition, the nonspecific distribution of nucleic acid drugs in normal cells remains

a problem in vivo.[21] Hence, developing efficient and targeted delivery systems for siRNA is an urgent need for RNAi-mediated therapy.

Nanotechnology has opened a new era for siRNA delivery to tumor tissues.[22,23] Nanocarriers could protect siRNA from digestion and improve delivery efficiency to cancer cells due to the enhanced permeability and retention (EPR) effect in tumor tissues.[24,25] Among various nanocarriers, protein nanocages attract considerable interest as an ideal platform because of their unique structural properties.[26,27] The protein nanocages have shown some advantages as drug nanocarriers, including monodisperse size, strictly ordered nanostructure, good biocompatibility and biodegradability, convenient functional interface (interior encapsulation, exterior display), easy modifications by genetic or chemical method.[28] Therefore, several proteins have been chosen to design siRNA delivery platform to tumor cells, such as ferritin,[29] thermosome,[30] small heat shock proteins (Hsp), [31] virus capsid proteins,[32] suggesting high efficiency for siRNA delivery.

In addition to the EPR effect, surface modification by peptides or antibodies could enhance the tumor-targeting delivery efficiency in some cancers expressing specific ligands or antigens.[33,34] For example, the overexpressed integrins ($\alpha_v\beta_3$ or $\alpha_v\beta_5$ subtype) in some solid tumors (for example, breast cancers, melanoma, glioma, and colorectal cancer cells) have been used to improve the drug delivery by introducing Arg-Gly-Asp (RGD) peptides on the surface of nanoparticles.[35] RGD-modified nanocarriers could be rapidly internalized into integrin-overexpressed cancer cells via

receptor-mediated endocytosis.[36,37] Moreover, cell-penetrating peptides (CPPs), a class of positively charged short peptides (less than 30 amino acids), could introduce a wide variety of cargos across the cell membrane into cells.[38] CPPs-modified nanocarriers have demonstrated an effective strategy to improve the cellular uptake of anticancer drugs for cancer therapy.[39]

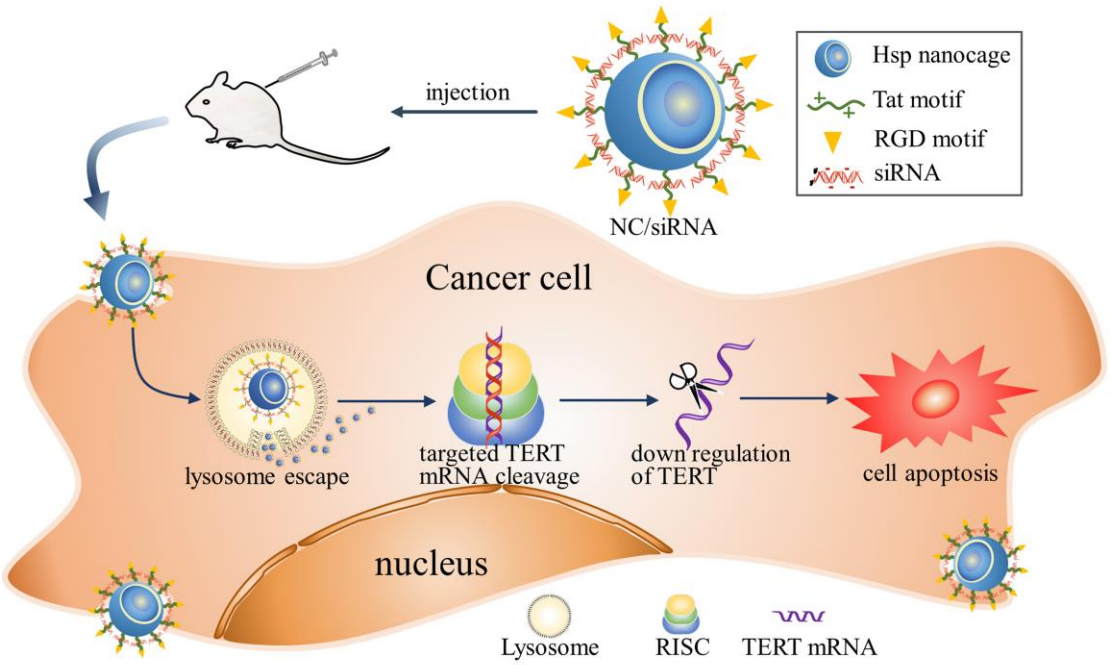

Scheme 1. Schematic illustration of preparation and mechanism of Hsp-Tat-RGD protein nanocage delivering siRNA targeting TERT in treatment of colorectal cancer.

Our previous study has shown that Hsp-R9 nanocage could efficiently transfect siRNA into cervical cancer cells and mediate green fluorescence protein (GFP) gene silencing in vitro.[31] To the best of our knowledge, most studies involving siRNA delivery by protein nanocages for cancer treatment were just performed in vitro. The actual effect of protein nanocage in mediating gene silence needs to be clarified in vivo. This study aims to design an efficient siRNA delivery system using protein

nanocage and investigate its role in siRNA-mediating gene silence for cancer therapy. Hsp protein nanocage, assembled by 24 subunits of Hsp monomer isolated from *Methanococcus jannaschii*, has an outer and inner diameter of 12 and 6.5 nm, respectively.[40] Hsp nanocages have satisfied stability even in harsh environments, including pH 5~11 or high temperature (up to 70 °C). In this study, Tat/RGD peptide co-decorated Hsp nanocage was prepared to build a stable and efficient siRNA delivery platform (Scheme 1). The siRNA condensing and protecting effect, cellular uptake, gene silencing assay, in vivo anticancer efficacy, and a safety assay were investigated in detail.

Experimental Section

Materials

Ampicillin sodium (Amp), Isopropyl β-D-thiogalactoside (IPTG), RNase A（60 U/mg), Imidazole, Ni-NTA Sefinose Resin, Unstained Protein Marker, *E. coli* DH5α, and BL21 (DE3) competent cells were all ordered from Sangon Biotech (China). 3,3'-dioctadecyloxacarbocyanine perchlorate (Dio), 2-(4-Amidinophenyl)-6-indolecarbamidine dihydrochloride (DAPI), and Lyso-Tracker Green were ordered from Beyotime (China). Cy3-maleimide was obtained from Kaixin Biotech. Annexin V-FITC apoptosis detection kit was ordered from Keygen Biotech (China). The Lipofectamine®3000 Reagent was ordered from Thermo Fisher Scientific. All types of siRNA, including negative control siRNA, siRNA targeting mTERT, and Cy3-labeled siRNA were ordered from Genepharma (China). The pET25b(+)/Hsp-Tat plasmid was constructed by Sangon Biotech (China).

Preparation and Characterization of Hsp-Tat and Hsp-Tat-RGD proteins

pET25b(+)/Hsp-Tat-RGD plasmid was constructed based on Hsp prokaryotic expression vector (pET25b(+)/Hsp), which was kindly gifted by the professor Masaharu Murata of the Department of Advanced Medical Initiatives, Faculty of Medical Science, Kyushu University (Japan). Both Hsp-Tat and Hsp-Tat-RGD proteins were prepared from *E. coli* BL21(DE3) cells and purified by Ni-NTA Sefinose Resin. Briefly, pET25b(+)/Hsp-Tat and pET25b(+)/Hsp-Tat-RGD plasmids were transformed into BL21(DE3) competent cells. The cells containing pET25b(+)/Hsp-Tat or pET25b(+)/Hsp-Tat-RGD plasmids were grown in Luria-Bertani (LB) medium containing 100 μg/ml ampicillin at 37°C. When the OD_{600} nm of culture reached 0.45 to 0.60, recombinant Hsp-Tat and Hsp-Tat-RGD proteins were expressed after adding IPTG at a final concentration of 1 mM for 6 h at 37°C. Subsequently, cells were collected by centrifugation and resuspended in Binding Buffer (20 mM Tris-HCl at pH 7.5, 500 mM NaCl, 20 mM imidazole, and 1 mM phenylmethanesulfonyl fluoride(PMSF)). The cell suspension was sonicated until the suspension became transparent; subsequently, the lysate was centrifuged at 7800 rpm for 20 min at 4°C. Recombinant proteins were purified from the supernatant using Ni-NTA Sefinose Resin. The resins were washed five times with washing buffer (20 mM Tris-HCl at pH 7.5, 500 mM NaCl, 5 mM imidazole) and eluted with elution buffer (20 mM Tris-HCl pH 7.5, 500 mM NaCl, 500 mM imidazole) three times. The elution solution was dialyzed against phosphate-buffered solution (PBS pH6.0). The

protein concentration was determined via BCA Protein Assay Kit (Sangon Biotech, China). The purified proteins were confirmed by 12% SDS-PAGE analysis.

The size distribution and zeta potential of HSP nanocages were determined by dynamic light scattering (DLS). Before the measurement, the lyophilized protein was dissolved in phosphate-buffered saline (PBS) (pH 6.0) and filtered through a 0.22 μm polyvinylidene fluoride (PVDF) filter. The size and potential of protein nanocages were measured at room temperature using a nanoparticle size and zeta potential meter (Microtrac, Nanotrac wave II). The morphology of protein nanocages was detected by transmission electron microscope (TEM) (JEOL JEM-1011).

Cell culture

Mouse colon carcinoma cells CT26 and mouse embryonic fibroblast cells NIH3T3 were maintained in Dulbecco's Modified Eagle Medium (DMEM) supplemented with 10% fetal bovine serum (FBS) (GIBCO) in a humidified atmosphere at 37°C and 5% CO_2.

Biocompatibility Studies

The biocompatibility of protein nanocages was examined by measuring the cell viability via MTT. Briefly, five thousand NIH 3T3 cells were seeded in each well of 96-well plates and incubated overnight. Subsequently, different concentrations of Hsp-Tat-RGD proteins (12.5, 25, 37.5, 50, and 100 μg/ml) were added to each well for 48 h of incubation. After four hours of incubation with MTT and the addition of

DMSO, the absorbance of cells at 490 nm was measured (TECAN, Spark 20M), and all experiments were performed in quadruplicate.

Preparation and Characterization of nanocage/siRNA complexes

A nonsense siRNA (20 bp) and Hsp-Tat-RGD protein were used to prepare nanocage/siRNA complexes. siRNA and nanocages were mixed in diethylpyrocarbonate (DEPC)-treated PBS buffer (pH 6.0) for one hour at 37°C. The chosen nitrogen/ phosphorus ratios were 0, 0.94, 1.88, 3.75, 7.5, 15, 30, 60 and 120 (protein/siRNA). The formation of nanocage/siRNA complexes was confirmed by agarose gel retardation assay. The siRNA-protecting assay was explored by measuring the undegraded siRNA after incubating with RNase. Free siRNA and Hsp-Tat-RGD NC/siRNA complexes were incubated with RNase A (final concentration 0.5 U/ml) at 37°C for one hour. The remaining siRNA was then detected by agarose gel electrophoresis. To examine the ability to resist the replacement of siRNA by a polyanion (heparin), we mixed Hsp-Tat-RGD NC/siRNA complexes (siRNA concentration: 2 μg/ml) with heparin sodium (54 mg/ml) in PBS buffer (pH 6.0) for one hour at 37°C. The chosen volume ratios were 0, 2, 4, 10, 40 and 80 (heparin/complexes). The released siRNA was detected by agarose gel electrophoresis. Stability analysis was tested using Hsp-Tat-RGD NC/siRNA complexes stored in FBS (37°C) and PBS (4°C). For the stability experiment in FBS, free siRNA and Hsp-Tat-RGD NC/siRNA complexes were mixed with FBS at a volume ratio of 1:1, respectively. Samples were incubated at 37°C for different times (0, 5, 10, 20, and 40 h) to release siRNA from the NC/siRNA complexes by heparin sodium. The released

siRNA was detected by agarose gel electrophoresis. For the stability experiment in PBS, Hsp-Tat-RGD NC/siRNA complexes in PBS (pH 6.0) were stored at 4°C for 7 days. The size of complexes on certain days was measured at room temperature using a nanoparticle size meter (NANOTRAC WAVE II, Microtrac).

Cellular uptake

The cellular uptake of Hsp-Tat-RGD NC was investigated by a confocal laser scanning microscope (CLSM). Cy3-labeled Hsp-Tat-RGD nanocages were prepared by conjugating Cyanine3 maleimide to the cysteine of Hsp protein according to the protocol (Kaixin Biotech). CT26 cells were seeded in 24-well plates containing slides for 24 h and treated with FAM-labeled Hsp-Tat-RGD NC (1 μM) for 1 h. The cells were fixed with 4% (w/v) paraformaldehyde for 20 min and stained with DAPI at 37°C for 10 min. CLSM images were captured via a confocal microscope (Carl Zeiss, LSM710) under the same conditions.

Cell transfection

The cell transfection analysis was investigated using Cy3-labeled siRNA (Genepharma) by CLSM imaging and flow cytometry assay. Briefly, the cells were seeded in a 24-well plate for 24 h of culture. The medium was replaced with fresh DMEM medium containing free siRNA, Lipo/siRNA complexes, Hsp-Tat NC/siRNA complexes, or Hsp-Tat-RGD NC/siRNA complexes for 24 h incubation. The cells were fixed with 4% paraformaldehyde, stained with DAPI, and imaged by CLSM under the same parameters. For flow cytometry analysis, the CT26 cells were incubated with free siRNA, Lipo/siRNA complexes, Hsp-Tat NC/siRNA complexes,

or Hsp-Tat NC/siRNA complexes for 24 h. The cells were processed with 0.25% trypsin for 1 min and collected by centrifuging. The cells were resuspended in PBS and analyzed by flow cytometry (ACEA Biosciences, NovoCyteTM).

Lysosome escape analysis

We used a lysosome-specific probe (Lyso-Tracker, green) and Cy3-labeled Hsp-Tat NC (red) for the lysosome escape assay. Briefly, the cells were incubated with Hsp-Tat-RGD NC for 2, 4, and 6 h. Lyso-Tracker (final concentration 50 nM) was added to each well, staining for 100 min at 37°C. After washing three times, the cells were fixed with 4% paraformaldehyde, stained with DAPI, and imaged by fluorescence microscope under the same parameters.

Western blot analysis

Mouse telomerase reverse transcriptase (mTERT) gene was chosen as the target gene of silencing. The sequences of siRNA targeting mTERT (Genepharma, China) were as follows:

siTERT 1: sense (5'-3') CAGCUGCUUAGGUCAUUCUTT, antisense (5'-3') AGAAUGACCUAAGCAGCUGTT; siTERT2: sense (5'-3') CAGAUCAAGAGCAGUAGUCTT, antisense (5'-3') GACUACUGCUCUUGAUCUGTT Briefly, the control group using PBS, the NC/siControl group using Hsp-Tat or Hsp-Tat-RGD protein nanocages, and the NC/TERT siRNA group using Hsp-Tat or Hsp-Tat-RGD protein nanocages were added to wells that were further incubated for 72 h after siRNA (80 nM) transfection.

The expression of mTERT protein was evaluated by Western blotting. Cells were lysed in lysis buffer for 30 min on ice. The protein concentration was determined using BCA Protein Assay Kit. An equal amount of protein was separated on the 8% SDS-PAGE, transferred onto PVDF membrane, blocked, and incubated overnight with monoclonal anti-TERT (Santa Cruz Biotechnology, USA) at a dilution of 1:1000. The protein antibody complexes were incubated with the HRP-labeled goat anti-mouse secondary antibody (Beyotime, China) at a dilution of 1:1000 for 2 h at room temperature and detected by BeyoECL Star chemiluminescence kit (Beyotime, China). As a loading control, β-actin was also assessed using an anti-mouse actin antibody (Beyotime, China). The grey value of each protein band was measured by Image Pro Plus (IPP) software for quantification. The relative TERT expression (%) was calculated according to the following formula: the gray value of TERT / the gray value of β-actin.

Cell apoptosis assay

Flow cytometry was conducted to measure the number of apoptotic cells. Briefly, free TERT siRNA, Lipo/siRNA complexes, Hsp-Tat NC/siRNA complexes, or Hsp-Tat-RGD NC/siRNA complexes were added to wells that were further incubated for 72 h after siRNA (80 nM) transfection. Subsequently, the cells were collected by centrifugation, washed, and resuspended in 500 μL of binding buffer. The cells were stained with annexin V-FITC and PI for 15 min at room temperature in the dark. The cells were analyzed using a flow cytometer (ACEA Biosciences, NovoCyteTM) within 60 min of staining.

In vivo anti-tumor efficacy

All animal studies were carried out according to the guidelines approved by the animal care and use committee of Beihua University. 6 week-old male BALB/c nude mice were divided into four groups with 5 mice in each group: PBS, free TERT siRNA2, Hsp-Tat NC/siTERT, and Hsp-Tat-RGD NC/siTERT group. CT26 tumors were induced in the mice by subcutaneously injecting CT26 cells (5.0×10^6) into the flank of the mice. Once the tumor volume reached approximately 70 mm^3, the mice were treated with PBS, free siRNA, Hsp-Tat NC/siRNA complexes, or Hsp-Tat-RGD NC/siRNA complexes. The day of the first drug injection was designed as day 0. The mice were administered five times via tail vein on days 0, 2, 4, 6, 8. siRNA was intravenously injected at a dose of 0.5 mg/kg body weight every two days for a total of five times. Body weights and tumor volumes were recorded every other day. The tumor volume was measured with calipers and calculated as follows: tumor volume (V) = (length) × $(width)^2/2$.

In vivo safety analysis

At the end of the treatment (day 20), all mice were sacrificed by cervical dislocation 2 days after the last treatment. Main organs (heart, liver, spleen, lung, and kidney) were isolated and preserved in 10% neutral-buffered formalin for two days. The tissues were then transformed into paraffin-embedded pathological sections for hematoxylin and eosin (H&E) staining.

Statistical analysis

All experiments were performed at least three times and expressed as means ± standard deviation (SD). All analysis was performed using the Statistical Program for Social Science (SPSS) for Windows. Two-tailed Student's t-tests and one-way ANOVAs were used to compare differences between paired and multiple groups, respectively. The results were considered statistically significant when *P <0.05, **P < 0.01, *** P < 0.001.

Results and Discussion

Preparation and characterization of Hsp-Tat-RGD nanocages

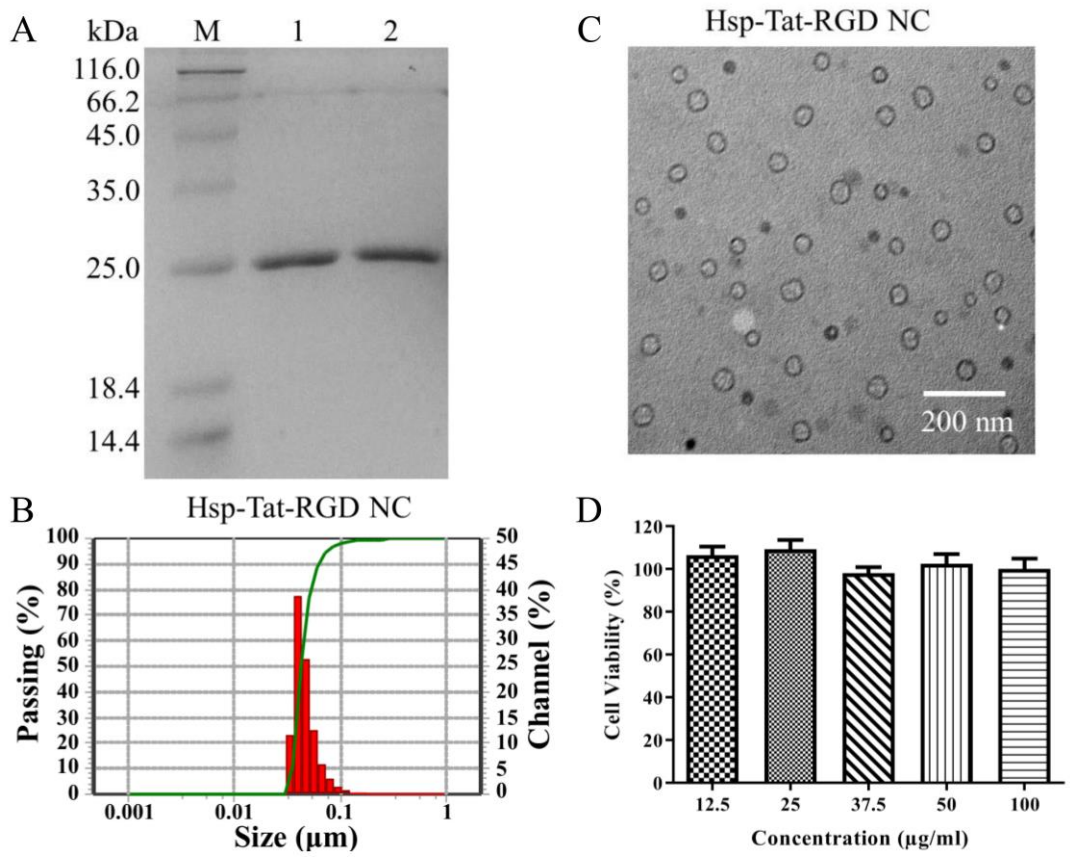

Figure 1. Preparation and characterization of Hsp-Tat-RGD NC. (A) SDS-PAGE analysis of purified Hsp-Tat and Hsp-Tat-RGD proteins. M: marker; lane 1: Hsp-Tat; lane 2: Hsp-Tat-RGD; (B) Size distribution analysis determined by dynamic light

scattering (DLS); (C) Morphology analysis of Hsp-Tat-RGD NC determined by transmission electron microscopy (TEM); (D) Biocompatibility analysis of Hsp-Tat-RGD NC in NIH3T3 cells.

Many reports have indicated that introducing short peptides at the C-terminus of the Hsp protein would not disrupt the main nanocage structure.[28] In this study, we introduced a relative DNA sequence corresponding to Tat peptide and RGD peptide to the C-terminus of the Hsp gene to construct the prokaryotic expression vector. The vector was transformed into competent *E. coli* cells (BL21) to produce Hsp-Tat-RGD fusion protein (Support Information, Figure S1). SDS-PAGE analysis indicated two protein bands with the predicted molecular weight of Hsp-Tat (23.28 kDa) and Hsp-Tat-RGD protein (23.76 kDa) (Figure 1A). The increased molecular weight of Hsp-Tat-RGD protein compared with Hsp could be attributed to the addition of RGD peptide and Tat peptide. The Hsp-Tat-RGD protein nanocage assembled by purified proteins has a mean size of 45.7 nm (Figure 1B) and -8.80 mV of surface charge (Support Information, Table 1). Compared with Hsp-Tat protein nanocage, the increased size of Hsp-Tat-RGD protein nanocage may be caused by the introduction of RGD sequence which displays on the outer surface of nanoparticle. The morphology analysis indicated a spherical hollow nanocage determined by transmission electron microscope (Figure 1C), consistent with the reported Hsp-derived nanoparticles.[41] We next investigated biocompatibility by measuring cell viability treated with protein nanocage. Human embryonic fibroblast cells (NIH3T3) were treated with different concentrations of Hsp-Tat-RGD proteins (ranging from

12.5 to 100 μg/ml) for two days. MTT results showed that protein nanocages have good biocompatibility with embryonic fibroblast cells in all tested concentrations (Figure 1D).

Preparation and characterization of Hsp-Tat-RGD NC/siRNA complexes

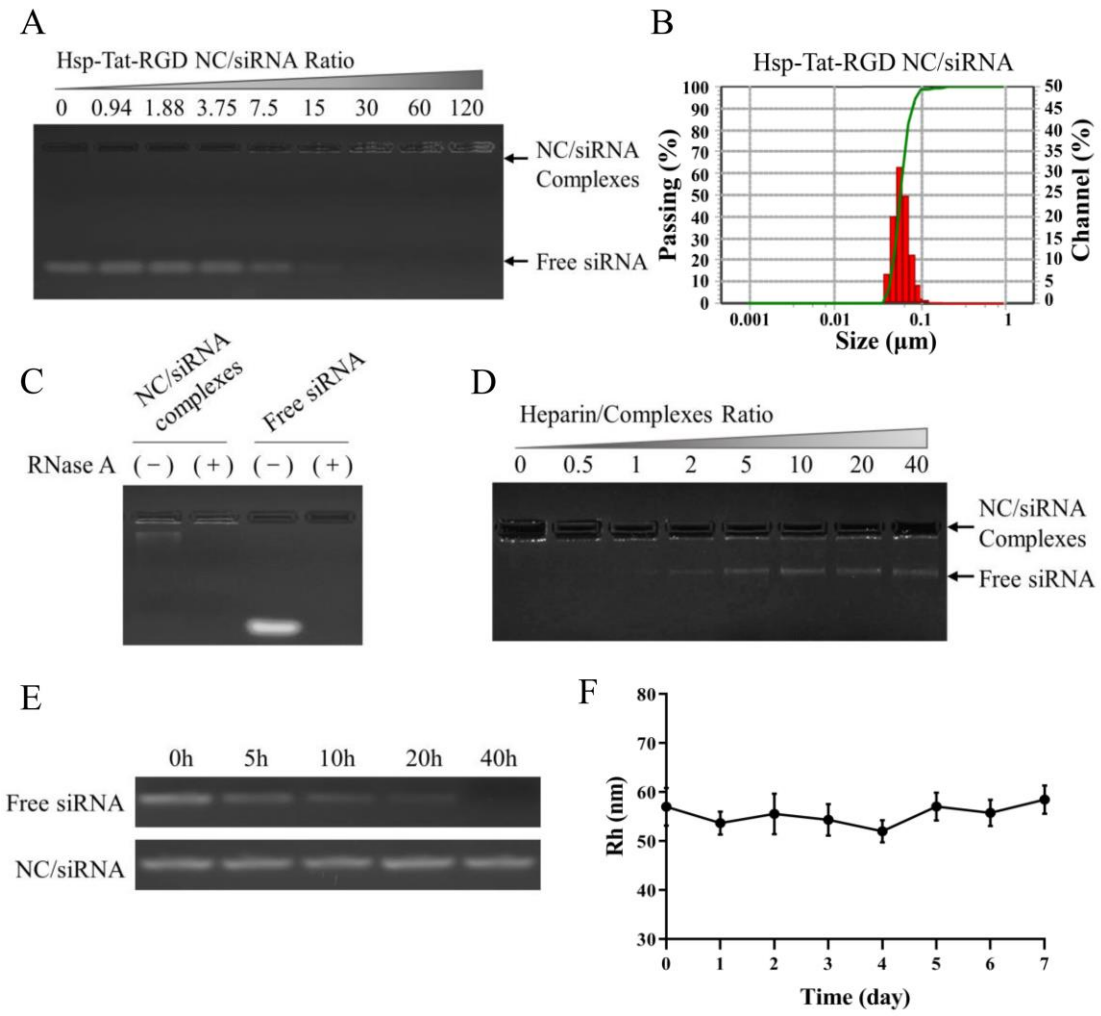

Figure 2. Characterization of Hsp-Tat-RGD NC/siRNA complexes in vitro. (A) siRNA condensing activity analysis of Hsp-Tat-RGD NC/siRNA complexes by gel retarded assay under different N/P ratios; (B) Size distribution analysis of Hsp-Tat-RGD NC/siRNA complexes determined by DLS; (C) Protecting effect of Hsp-Tat-RGD NC on siRNA from RNase; (D) Heparin decomplexation assay of NC/siRNA complexes; (E) Stability analysis of Hsp-Tat-RGD NC/siRNA complexes

at varying incubating hours with FBS; (F) Size changes of Hsp-Tat-RGD NC complexes at varying incubating days with PBS.

To evaluate the siRNA condensing ability of Hsp-Tat-RGD NC, we then mixed the NC with siRNA at varying nitrogen/phosphate (N/P) ratios (the ratio of amine groups on protein to phosphates on siRNA). The siRNA condensing activity was determined by measuring the reduced migration of NC/siRNA complexes in agarose gel (gel retarded assay). As shown in Figure 2A, free siRNA migration was gradually reduced by Hsp-Tat-RGD NC with the increasing N/P ratio, which was wholly halted at an N/P ratio of 30 or higher, suggesting the formation of NC/siRNA complexes. We then prepared Hsp-Tat-RGD NC/siRNA complexes at the fixed N/P ratio of 30 for other experiments. These complexes have a mean size of 55.8 nm and a zeta potential value of -9.22 mV (Figure 2B). The increased size of complexes than nanocage was caused by the binding of negatively charged siRNA with positively charged TAT motif via electrostatic adsorption.

The protecting effect of Hsp-Tat-RGD NC was determined by detecting the remaining siRNA after RNase treatment. After one hour treatment with RNase, no residual siRNA was observed in free siRNA group, while no noticeable siRNA degradation was observed in NC/siRNA complexes group (Figure 2C). These results demonstrated that compared with easily digested free siRNA, NC/siRNA complexes could protect the condensed siRNA from RNase degradation. In a heparin de-complex assay, siRNA was readily de-complexed and released from Hsp-Tat-RGD NC with the increasing heparin concentration (Figure 2D), suggesting good siRNA release.

The stability of NC/siRNA complexes was determined by measuring the residual content of siRNA after incubation in fetal bovine serum (FBS) and the size changes in

phosphate-buffered saline (PBS) over time. After incubating with FBS for various time lengths, the residual siRNA in complexes was detected by gel electrophoresis. Compared with no residual siRNA observed in free siRNA group, there was no noticeable siRNA degradation in the NC/siRNA complexes group after 40 hours of FBS treatment (Figure 2E), suggesting the good stability of NC/siRNA complexes in FBS. Moreover, no apparent size change of NC/siRNA complexes was detected in PBS after seven days of treatment (Figure 2F). These results showed that the stable complexes formed by Hsp-Tat-RGD NC and siRNA could protect the complexed siRNA from degradation.

Cellular uptake and lysosomal escape

The cellular uptake of Hsp-Tat-RGD/siRNA complexes was examined using Cy3-labeled siRNA in colorectal cancer cells by confocal laser scanning microscope (CLSM). To track the intracellular localization in CT26 cells, both Hsp-Tat NC and Hsp-Tat-RGD NC was labeled with the fluorescent dye Cyanine3 (Cy3) to get a red fluorescent nanoparticle. An apparent red-spotted distribution of nanocages was observed in the perinuclear region, while Hsp-Tat-RGD NC showed a higher fluorescent intensity than Hsp-Tat NC (Figure 3A). These results showed that RGD-modification enhanced the cellular uptake of Cy3-labeled nanocages in caner cells. We next explored the lysosomal escape of Hsp-Tat-RGD NC using a green lysosome probe (Lyso-Tracker). The merged yellow fluorescence (arrowhead) was detected after 4 h incubation (Figure 3B), suggesting the co-localization of Cy3-labeled protein nanocages with lysosomes. Extending the incubation time to 6 h permitted the escape of nanocages from lysosomes (Figure 3B), suggesting a good lysosome escape property.

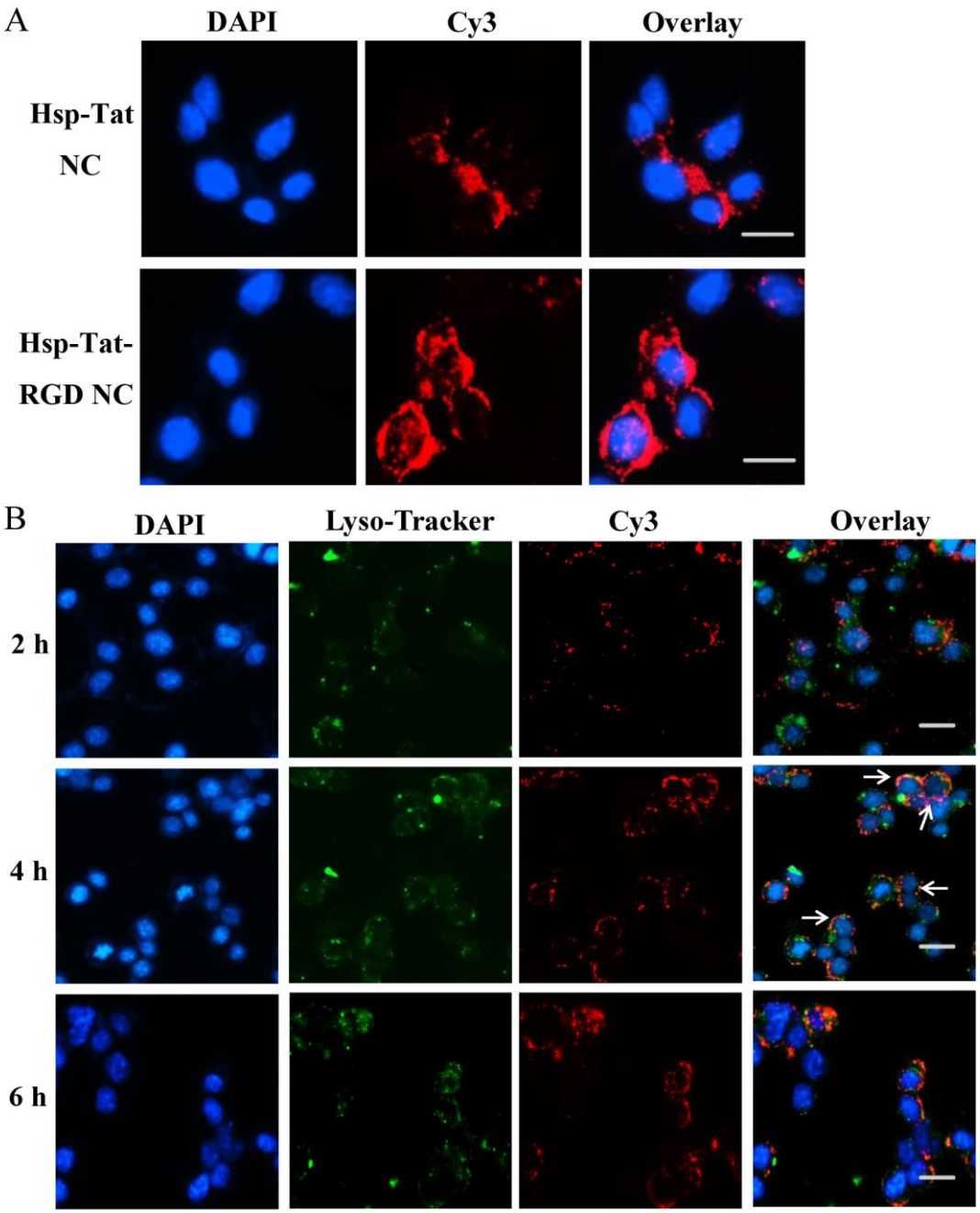

Figure 3. Cellular uptake and lysosomal escape of Hsp-Tat-RGD nanocages in CT26 cells by CLSM. (A) Cellular uptake of Cy3-labeled Hsp-Tat NC and Hsp-Tat-RGD NC after 2 h of incubation; (B) Lysosome escape analysis of Hsp-Tat-RGD NC complexes after 4 h of incubation. Nuclei were stained with DAPI (blue); the red fluorescence indicated Cy3-labeled nanocages; the lysosome was stained with Lyso-Tracker (green). Scale bars: 20 μm.

siRNA transfection analysis by Hsp-Tat-RGD nanocages

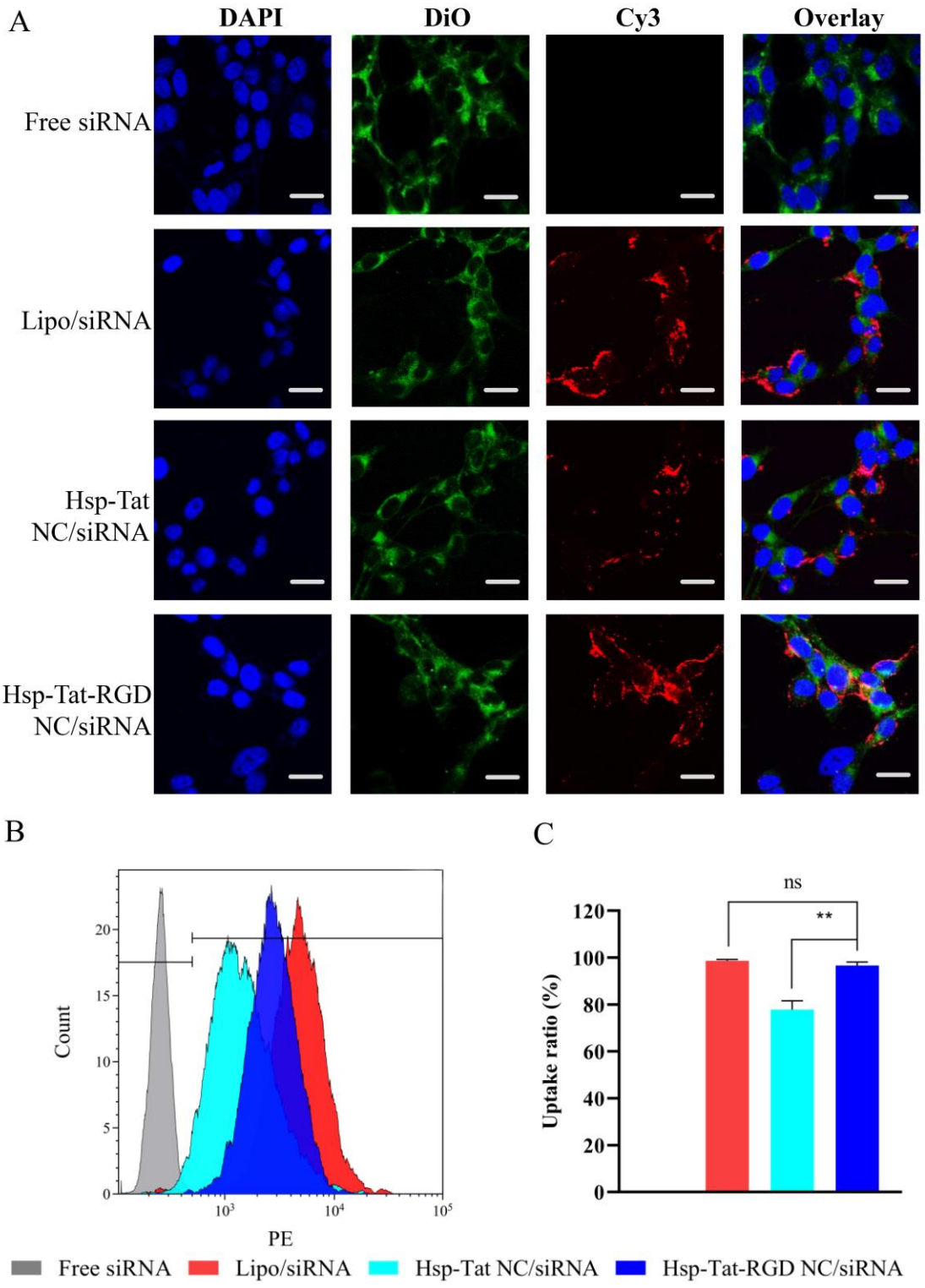

Figure 4. siRNA transfection analysis of Hsp-Tat-RGD NC in CT26 cells. (A) siRNA transfection analysis by CLSM imaging using Cy-3 labeled siRNA; (B) Flow

cytometry analysis of CT26 cells treated with Hsp-Tat-RGD NC/siRNA complexes; (C) Uptake rate analysis via flow cytometry. The nucleus was stained by DAPI (blue signal), the cell membrane was stained by Dio (green signal), and Cy3-labeled siRNA was used (red signal).

We next explored the siRNA transfection ability of Hsp-Tat-RGD NC using Cy3-labeled siRNA in CT26 cells. Lipofectamine 3000 (Lipo), a commercial transfection reagent, was used as a positive control for siRNA transfection. The results showed no detected siRNA distribution in CT26 cells treated with free siRNA group, while successful siRNA transfection was detected in Lipo/siRNA, Hsp-Tat NC/siRNA, and Hsp-Tat-RGD NC/siRNA group (Figure 4A). As for two protein nanocages, Hsp-Tat-RGD NC transfected more siRNA (96.6%) into CT26 cells than Hsp-Tat NC (77.8%) (Figure 4B and 4C), showing an enhanced siRNA transfection ability of RGD-decorated nanocages. The increased siRNA internalization may be attributed to improved uptake of Hsp-Tat-RGD nanocages in integrin-overexpressed cancer cells.[42,43]

Gene silencing effect of Hsp-Tat-RGD/siTERT complexes

To evaluate the gene silencing effect, we chose mouse TERT gene and designed two targeting siRNA (named siTERT1 and siTERT2) for exploring RNAi effects in CT26 cells(Support Information, Figure S2 and S3). The results showed that Hsp-Tat-RGD NC/siRNA complexes and Hsp-Tat NC/siRNA complexes could significantly reduce the TERT expression in CT26 cells using siTERT1 or siTERT2 (Figure 5A). Using siTERT1 or siTERT2, Hsp-Tat-RGD NC showed a higher inhibition effect than Hsp-Tat NC in regulating TERT expression (Figure 5B). The enhanced gene silencing

could be explained that more siRNA distribution in cancer cells treated with Hsp-Tat-RGD NC downregulated TERT expression than that in Hsp-Tat NC group.

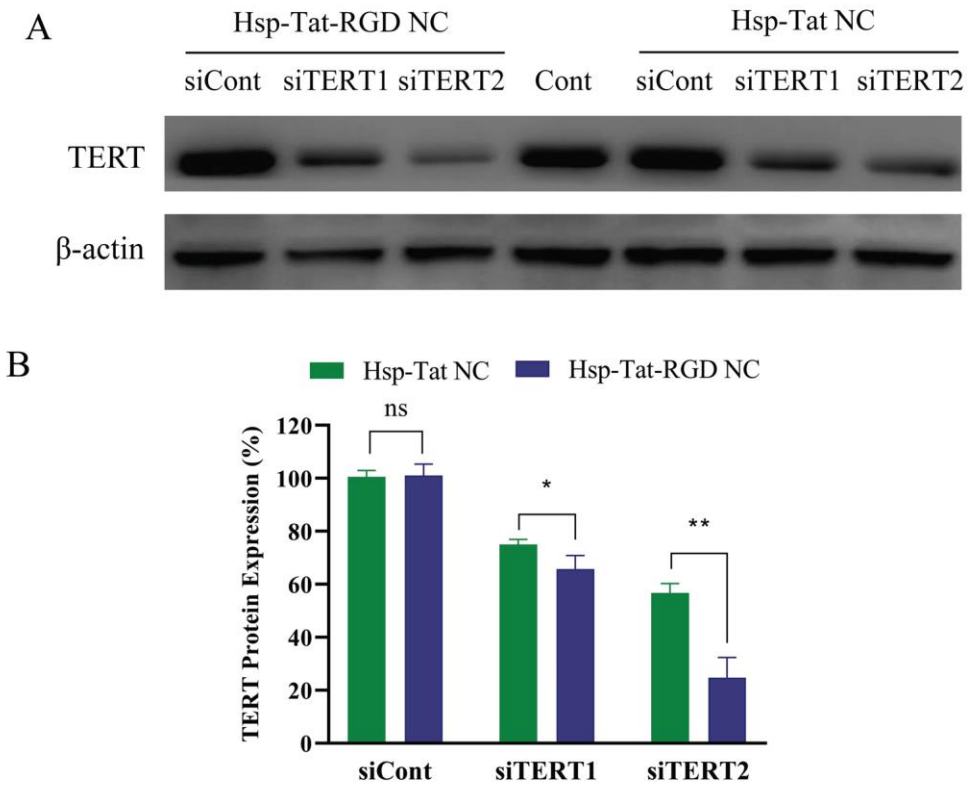

Figure 5. Gene silencing effect of Hsp-Tat-RGD/siTERT complexes in CT26 cells. (A) Downregulation of TERT expression by different formulations via western blot analysis. β-actin is used as the negative control unaffected by siRNA-induced gene silencing. (B) Quantitation analysis of relative TERT protein expression normalized to β-actin. Grey values of each protein band in western blot were determined by Image-Pro Plus (IPP) software.

Pro-apoptotic effect induced by Hsp-Tat-RGD/siTERT complexes

Considering the essential role of TERT gene in maintaining telomere structure in tumor growth, we then examined the pro-apoptotic effect of Hsp-Tat-RGD/siTERT complexes in CT26 cells. Nearly no cell apoptosis was observed in control and free siRNA groups, Lipo, Hsp-Tat, and Hsp-Tat-RGD nanocarriers delivering siTERT

triggered apparent cell apoptosis in CT26 cells (Figure 6A). As for two protein nanocages, Hsp-Tat-RGD/siTERT2 triggered more cell death (47.81%) than Hsp-Tat/siTERT2 (35.19%) in CT26 cells. A similar pro-apoptotic tendency was observed in siTERT1-treated groups (Figure 6B). Notably, the apoptosis rate in Hsp-Tat-RGD/siTERT2 group was nearly 1.5-fold higher than that in the Lipo/siTERT2 group (Figure 6C), suggesting a robust pro-apoptotic ability of Hsp-Tat-RGD/siTERT2 complexes.

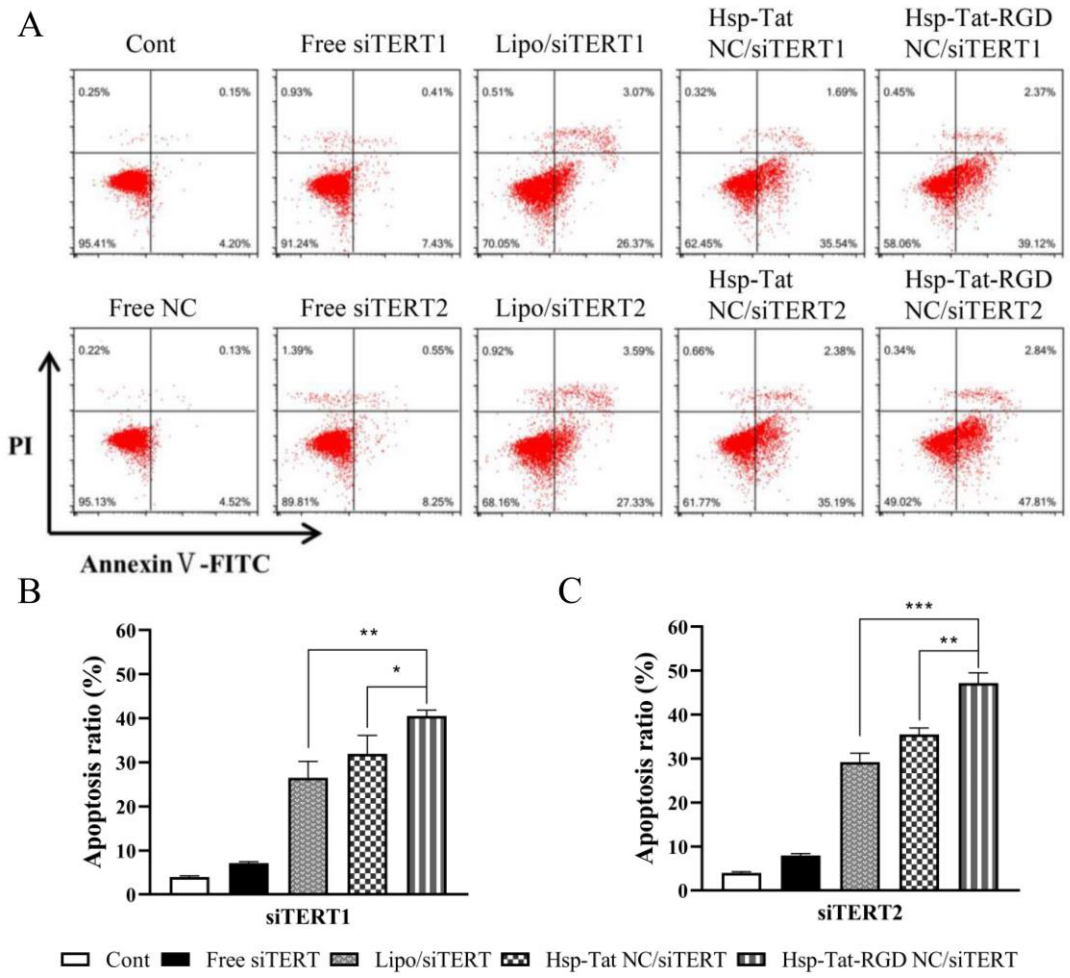

Figure 6. The pro-apoptotic effect of Hsp-Tat-RGD NC delivering siTERT in CT26 cell. (A) The cell apoptosis induced by different formulations was investigated by flow cytometry analysis. (B) Statistical analysis of the apoptosis rate by free siRNA, Lipo, Hsp-Tat NC, and Hsp-Tat-RGD NC using siTERT1. (C) Statistical analysis of

the apoptosis rate by free siRNA, Lipo, Hsp-Tat NC, and Hsp-Tat-RGD NC using siTERT2.

In vivo antitumor efficacy of Hsp-Tat-RGD/siTERT complexes

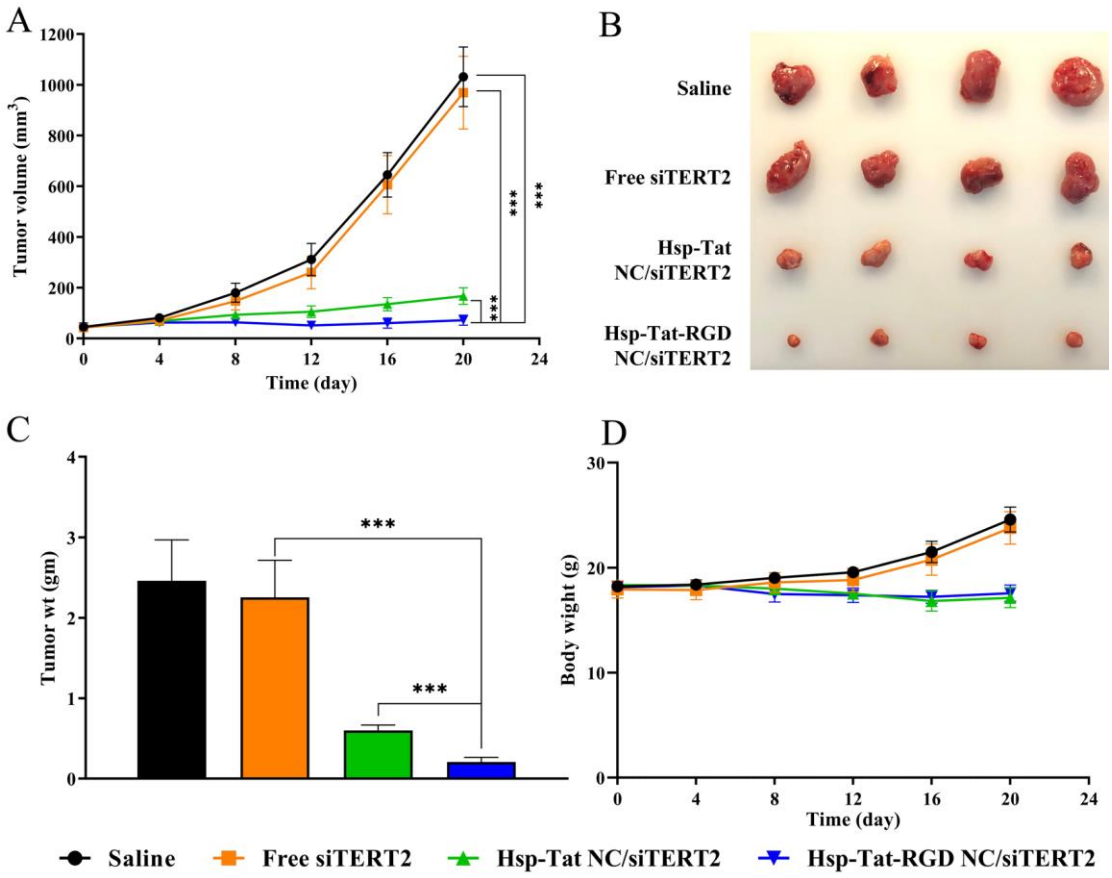

Figure 7. In vivo antitumor efficacy analysis of Hsp-Tat-RGD/siTERT complexes on the CT26 xenograft. (A) Average tumor volumes over time; (B) The images of excised tumors from mice treated with saline, free siTERT2, Hsp-Tat/siTERT complexes and Hsp-Tat-RGD/siTERT complexes on day 20; (C) Average excised tumor weight on day 20; (D) Average body weights over time.

To assess the systemic antitumor effect of Hsp-Tat-RGD/siTERT complexes in vivo, we established mice bearing subcutaneous tumor xenograft using CT26 cells. We applied saline, free siTERT2, Hsp-Tat/siTERT complexes, or Hsp-Tat-RGD/siTERT

complexes to explore the antitumor efficacy in vivo. The day of the first drug injection was designed as day 0. The mice were administered five times via tail vein on days 0, 2, 4, 6, 8. The results showed that the average tumor volumes of mice treated with Hsp-Tat-RGD/siTERT2 or Hsp-Tat/siTERT2 were significantly smaller than the control group on day 20 (Figure 7A). Compared with Hsp-Tat/siTERT2, Hsp-Tat-RGD/siTERT2 demonstrated a superior antitumor efficacy on the CT26 xenograft (Figure 7A). On day 20, the tumors were excised from mice and weighed. The xenografts from the mice treated with Hsp-Tat-RGD/siTERT2 were significantly reduced compared with the Hsp-Tat group (Figure 7B and 7C). The enhanced tumor inhibition of Hsp-Tat-RGD/siTERT could be attributed to the enhanced tumor cell apoptosis in CT26 cells. Moreover, the body weight assay showed no apparent body weight loss during the treatments (Figure 7D).

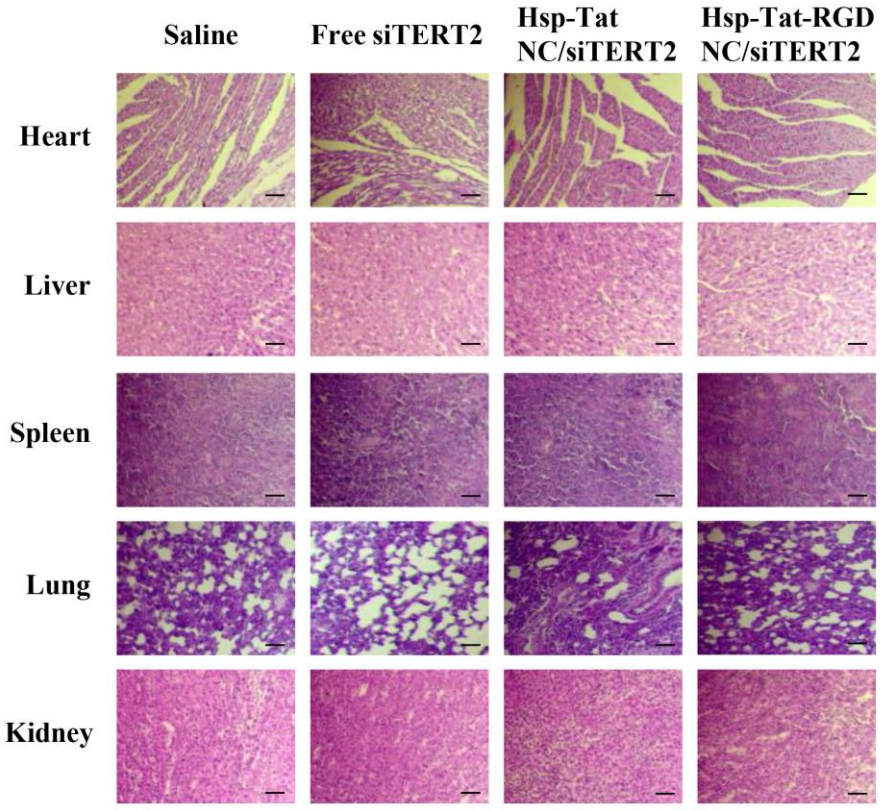

Figure 8. Safety analysis of Hsp-Tat-RGD/siTERT complexes in CT26-xenograft mice. Ex vivo hematoxylin and eosin (H&E) staining of main organs including heart, liver, spleen, lung, and kidney. Scale bar: 100 μm.

Safety concerns are also investigated in this study via pathology examination. On day 20, main organs (including heart, liver, spleen, lung, and kidney) were isolated from mice and transformed into frozen slices. The hematoxylin and eosin (H&E) staining slices were used to determine the safety concerns of different formulations. No apparent inflammation and tissue damage were observed in the slice of Hsp-Tat/siTERT or Hsp-Tat-RGD/siTERT group, suggesting good safety of Hsp protein nanocages in transfecting siRNA in vivo.

Conclusion

In summary, we developed Hsp-Tat-RGD protein nanocage as an efficient and safe delivery system to deliver siTERT into colorectal cancer cells for cancer therapy. Hsp-Tat-RGD NC showed improved cellular uptake and increased siRNA transfection in integrin-overexpressed CT26 cells. Hsp-Tat-RGD delivering siTERT could substantially inhibit the TERT expression and trigger cell apoptosis in CT26 cells. Moreover, Hsp-Tat-RGD/siTERT demonstrates enhanced antitumor efficacy in mice with CT26 xenograft. Our study suggests that Hsp-Tat-RGD NC may have a great potential for applications in gene-related therapies in the future.

Supporting Information

The Supporting Information is available free of charge at https://pubs.acs.org/doi/XX

Amino acid sequences of Hsp-Tat and Hsp-Tat-RGD proteins, particle sizes and zeta potentials of nanocages and complexes, prokaryotic expression and purification of Hsp-Tat-RGD protein, TERT gene silence by different siRNA concentrations in this work (PDF).

Corresponding author：

Xingang Guan - Medical School, Taizhou University, 1139 Shifu Avenue, Taizhou 318000, PR China; College of Medical Technology, Beihua University, 3999 East Binjiang Road, Jilin 132013, PR China; orcid.org/ 0000-0003-3776-1818. Email: guanxg@ciac.ac.cn

Authors:

Hao Wang - Medical School, Taizhou University, 1139 Shifu Avenue, Taizhou 318000, PR China; College of Medical Technology, Beihua University, 3999 East Binjiang Road, Jilin 132013, PR China;

Ning Liu - College of Medical Technology, Beihua University, 3999 East Binjiang Road, Jilin 132013, PR China;

Fuxu Yang - Medical School, Taizhou University, 1139 Shifu Avenue, Taizhou 318000, PR China; College of Medical Technology, Beihua University, 3999 East Binjiang Road, Jilin 132013, PR China;

Nannan Hu - Medical School, Taizhou University, 1139 Shifu Avenue, Taizhou 318000, PR China; College of Medical Technology, Beihua University, 3999 East Binjiang Road, Jilin 132013, PR China;

Mingyue Wang - College of Medical Technology, Beihua University, 3999 East Binjiang Road, Jilin 132013, PR China;

Meiying Cui - College of Medical Technology, Beihua University, 3999 East Binjiang Road, Jilin 132013, PR China;

Nico Bruns - Department of Pure and Applied Chemistry, University of Strathclyde, Glasgow G1 1XL, UK

Conflict of interest

The authors declare no conflict of interest.

Acknowledgements

The authors thank Prof. Masaharu Murata in Kyushu University (Japan) for his generous gift of HSP16.5 plasmid. This study was supported by the National Natural Science Foundation of China (No. 51503003).

References

(1) Siegel, R. L.; Miller, K. D.; Goding Sauer, A.; Fedewa, S. A.; Butterly, L. F.; Anderson, J. C.; Cercek, A.; Smith, R. A.; Jemal, A. Colorectal Cancer Statistics, 2020. *CA-Cancer J. Clin.* **2020,** *70* (3), 145-164.

(2) Force, U.; Bibbins-Domingo, K.; Grossman, D.; Curry, S.; Davidson, K.; Epling, J.; Garcia, F.; Gillman, M.; Harper, D.; Kemper, A. Screening for Colorectal Cancer. *JAMA* **2016,** *315*, 2564-2575.

(3) Schreuders, E. H.; Ruco, A.; Rabeneck, L.; Schoen, R. E.; Sung, J. J.; Young, G. P.; Kuipers, E. J. Colorectal Cancer Screening: A Global Overview of Existing Programmes. *Gut* **2015,** *64* (10), 1637-1649.

(4) Ganesh, K.; Stadler, Z. K.; Cercek, A.; Mendelsohn, R. B.; Shia, J.; Segal, N. H.; Diaz, L. A. Immunotherapy in Colorectal Cancer: Rationale, Challenges And Potential. *Nat. Rev. Gastro. Hepat.* **2019,** *16* (6), 361-375.

(5) M McQuade, R.; Stojanovska, V.; C Bornstein, J.; Nurgali, K. Colorectal Cancer Chemotherapy: the Evolution of Treatment and New Approaches. *Curr. Med. Chem.* **2017,** *24* (15), 1537-1557.

(6) Chen, X.; Mangala, L. S.; Rodriguez-Aguayo, C.; Kong, X.; Lopez-Berestein, G.; Sood, A. K. RNA Interference-Based Therapy and its Delivery Systems. *Cancer Metast. Rev.* **2018,** *37* (1), 107-124.

(7) Jafri, M. A.; Ansari, S. A.; Alqahtani, M. H.; Shay, J. W. Roles of Telomeres and Telomerase in Cancer, and Advances in Telomerase-Targeted Therapies. *Genome Med.* **2016,** *8* (1), 1-18.

(8) Shay, J. W.; Wright, W. E. Telomeres and Telomerase: Three Decades of Progress. *Nat. Rev. Genet.* **2019,** *20* (5), 299-309.

(9) Ruden, M.; Puri, N. Novel Anticancer Therapeutics Targeting Telomerase. *Cancer Treat. Rev.* **2013,** *39* (5), 444-456.

(10) Hannen, R.; Bartsch, J. W. Essential Roles of Telomerase Reverse Transcriptase hTERT in Cancer Stemness and Metastasis. *FEBS lett.* **2018,** *592* (12), 2023-2031.

(11) Leão, R.; Apolónio, J. D.; Lee, D.; Figueiredo, A.; Tabori, U.; Castelo-Branco, P. Mechanisms of Human Telomerase Reverse Transcriptase (hTERT) Regulation: Clinical Impacts in Cancer. *J. Biomed. Sci.* **2018,** *25* (1), 1-12.

(12) Khattar, E.; Kumar, P.; Liu, C. Y.; Akıncılar, S. C.; Raju, A.; Lakshmanan, M.; Maury, J. J. P.; Qiang, Y.; Li, S.; Tan, E. Y. Telomerase Reverse Transcriptase Promotes Cancer Cell Proliferation by Augmenting tRNA Expression. *J. Clin. Invest.* **2016,** *126* (10), 4045-4060.

(13) Liu, T.; Yuan, X.; Xu, D. Cancer-Specific Telomerase Reverse Transcriptase (TERT) Promoter Mutations: Biological and Clinical Implications. *Genes* **2016,** *7* (7), 38.

(14) McKelvey, B. A.; Umbricht, C. B.; Zeiger, M. A. Telomerase Reverse Transcriptase (TERT) Regulation in Thyroid Cancer: A Review. *Front. Endocrinol.* **2020,** *11*, 485.

(15) Rampazzo, E.; Del Bianco, P.; Bertorelle, R.; Boso, C.; Perin, A.; Spiro, G.; Bergamo, F.; Belluco, C.; Buonadonna, A.; Palazzari, E. The Predictive and Prognostic Potential of Plasma Telomerase Reverse Transcriptase (TERT) RNA in Rectal Cancer Patients. *Brit. J. Cancer* **2018,** *118* (6), 878-886.

(16) Maida, Y.; Masutomi, K. Telomerase Reverse Transcriptase Moonlights: Therapeutic Targets Beyond Telomerase. *Cancer Sci.* **2015,** *106* (11), 1486-1492.

(17) Wilson, R. C.; Doudna, J. A. Molecular Mechanisms of RNA Interference. *Annu. Rev. Biophys.* **2013,** *42*, 217-239.

(18) Pecot, C. V.; Calin, G. A.; Coleman, R. L.; Lopez-Berestein, G.; Sood, A. K. RNA Interference in The Clinic: Challenges and Future Directions. *Nat. Rev. Cancer* **2011,** *11* (1), 59-67.

(19) Saw, P. E.; Song, E.-W. siRNA Therapeutics: A Clinical Reality. Sci. China Life Sci. **2020,** *63* (4), 485-500.

(20) Aghamiri, S.; Raee, P.; Talaei, S.; Mohammadi-Yeganeh, S.; Bayat, S.; Rezaee, D.; Ghavidel, A. A.; Teymouri, A.; Roshanzamiri, S.; Farhadi, S. Nonviral siRNA

Delivery Systems for Pancreatic Cancer Therapy. *Biotechnol. Bioeng.* **2021**, 118 (10), 3669-3690.

(21) Hu, B.; Zhong, L.; Weng, Y.; Peng, L.; Huang, Y.; Zhao, Y.; Liang, X.-J. Therapeutic siRNA: State of the Art. *Signal Transduct. Tar.* **2020**, 5 (1), 1-25.

(22) Xin, Y.; Huang, M.; Guo, W. W.; Huang, Q.; zhen Zhang, L.; Jiang, G. Nano-Based Delivery of RNAi in Cancer Therapy. Mol. Cancer **2017,** *16* (1), 1-9.

(23) Kim, H. J.; Kim, A.; Miyata, K.; Kataoka, K. Recent Progress in Development of siRNA Delivery Vehicles for Cancer Therapy. *Adv. Drug Delivery Rev.* **2016,** *104*, 61-77.

(24) Zhang, P.; An, K.; Duan, X.; Xu, H.; Li, F.; Xu, F. Recent Advances in siRNA Delivery for Cancer Therapy Using Smart Nanocarriers. *Drug Discov. Today* **2018,** *23* (4), 900-911.

(25) Lee, E. J.; Lee, N. K.; Kim, I. S. Bioengineered Protein-Based Nanocage for Drug Delivery. *Adv. Drug Deliv. Rev.* **2016,** *106* (Pt A), 157-171.

(26) Wang, Y.; Douglas, T. Protein Nanocage Architectures for the Delivery of Therapeutic Proteins. *Curr. Opin. Colloid Interface Sci.* **2021,** *51*, 101395.

(27) Edwardson, T. G. W.; Hilvert, D. Virus-Inspired Function in Engineered Protein Cages. *J. Am. Chem. Soc.* **2019,** *141* (24), 9432-9443.

(28) Cannon, K. A.; Ochoa, J. M.; Yeates, T. O. High-Symmetry Protein Assemblies: Patterns and Emerging Applications. *Curr. Opin. Struct. Biol.* **2019,** *55*, 77-84.

(29) Pediconi, N.; Ghirga, F.; Del Plato, C.; Peruzzi, G.; Athanassopoulos, C. M.; Mori, M.; Crestoni, M. E.; Corinti, D.; Ugozzoli, F.; Massera, C. Design and Synthesis of Piperazine-Based Compounds Conjugated to Humanized Ferritin as Delivery System of siRNA in Cancer Cells. *Bioconjugate Chem.* **2021,** *32* (6), 1105–1116.

(30) Nussbaumer, M. G.; Duskey, J. T.; Rother, M.; Renggli, K.; Chami, M.; Bruns, N. Chaperonin-Dendrimer Conjugates for siRNA Delivery. *Adv. Sci.* **2016,** *3* (10), 1600046.

(31) Guan, X.; Chang, Y.; Sun, J.; Song, J.; Xie, Y. Engineered Hsp Protein Nanocages for siRNA Delivery. *Macromol. Biosci.* **2018,** *18* (5), e1800013.

(32) Pretto, C.; van Hest, J. C. Versatile Reversible Cross-Linking Strategy to Stabilize CCMV Virus Like Particles for Efficient siRNA Delivery. *Bioconjugate Chem.* **2019,** *30* (12), 3069-3077.

(33) Dong, Y.; Yu, T.; Ding, L.; Laurini, E.; Huang, Y.; Zhang, M.; Weng, Y.; Lin, S.; Chen, P.; Marson, D. A Dual Targeting Dendrimer-Mediated siRNA Delivery System for Effective Gene Silencing in Cancer Therapy. *J. Am. Chem. Soc.* **2018,** *140* (47), 16264-16274.

(34) Attia, M. F.; Anton, N.; Wallyn, J.; Omran, Z.; Vandamme, T. F. An Overview of Active and Passive Targeting Strategies to Improve the Nanocarriers Efficiency to Tumour Sites. *J. Pharm. Pharmacol.* **2019**, 71 (8), 1185-1198.

(35) Yu, Y.-P.; Wang, Q.; Liu, Y.-C.; Xie, Y. Molecular Basis for the Targeted Binding of RGD-Containing Peptide to Integrin αVβ3. *Biomaterials* **2014,** *35* (5), 1667-1675.

(36) Alzamely, K. O.; Hajizadeh, F.; Heydari, M.; Sede, M. J. G.; Asl, S. H.; Peydaveisi, M.; Masjedi, A.; Izadi, S.; Nikkhoo, A.; Atyabi, F. Combined Inhibition of CD73 and ZEB1 by Arg-Gly-Asp (RGD)-Targeted Nanoparticles Inhibits Tumor Growth. *Colloid. Surface. B* **2021,** *197*, 111421.

(37) Fu, S.; Xu, X.; Ma, Y.; Zhang, S.; Zhang, S. RGD Peptide-Based Non-Viral Gene Delivery Vectors Targeting Integrin αvβ3 for Cancer Therapy. *J. Drug. Target.* **2019,** *27* (1), 1-11.

(38) Xie, J.; Bi, Y.; Zhang, H.; Dong, S.; Teng, L.; Lee, R. J.; Yang, Z. Cell-Penetrating Peptides in Diagnosis and Treatment of Human Diseases: from Preclinical Research to Clinical Application. *Front. Pharmacol.* **2020,** *11*, 697.

(39) Silva, S.; Almeida, A. J.; Vale, N. J. B. Combination of Cell-Penetrating Peptides with Nanoparticles for Therapeutic Application: A Review. *Biomolecules* **2019,** *9* (1), 22.

(40) Wang, D.; Chen, L.; Wang, M.; Cui, M.; Huang, L.; Xia, W.; Guan, X. Delivering Proapoptotic Peptide by HSP Nanocage for Cancer Therapy. *Macromol. Chem. Phys.* **2020,** *221* (12), 2000003.

(41) Kawano, T.; Murata, M.; Piao, J. S.; Narahara, S.; Hamano, N.; Kang, J.-H.; Hashizume, M. Systemic Delivery of Protein Nanocages Bearing CTT Peptides for Enhanced Imaging of MMP-2 Expression in Metastatic Tumor Models. *Int. J Mol. Sci.* **2015,** *16* (1), 148-158.

(42) Garanti, T.; Alhnan, M. A.; Wan, K.-W. RGD-decorated Solid Lipid Nanoparticles Enhance Tumor Targeting, Penetration and Anticancer Effect of Asiatic Acid. *Nanomedicine-UK* **2020,** *15* (16), 1567-1583.

(43) Wang, Z.; Zhang, S.; Zhang, R.; Chen, X.; Sun, G.; Zhou, M.; Han, Q.; Zhang, B.; Zhao, Y.; Jiang, B. Bioengineered Dual-Targeting Protein Nanocage for Stereoscopically Loading of Synergistic Hydrophilic/Hydrophobic Drugs to Enhance Anticancer Efficacy. *Adv. Funct. Mater.* **2021**, 2102004.